Research Article | Vol. 9, No. 9 / 1 September 2019 / Optical Materials Express 3717
Optical Materials EXPRESS

# Asymmetric hysteresis in vanadium dioxide thin films

MARC CURRIE,[1,*] VIRGINIA D. WHEELER,[1] BRIAN DOWNEY,[1] NEERAJ NEPAL,[1] SYED B. QADRI,[1] JAMES A. WOLLMERSHAUSER,[1] JASON AVILA,[2] AND LUKE NYAKITI[3]

[1]U.S. Naval Research Laboratory, Washington, DC 20375, USA
[2]ASEE Postdoctoral Fellow, 1818 N. Street NW, Washington, DC 20036, USA
[3]Dept. Material Science and Engineering, Texas A&M University, College Station, TX 77843, USA
[*]marc.currie@nrl.navy.mil

**Abstract:** Vanadium dioxide is a material that undergoes phase changes and switches between metallic and insulating states, thereby producing dramatic changes in optical properties. This transition is a reversible but hysteretic process, which is investigated here as a function of atomic layer deposited film thickness. Increasing the thickness of vanadium dioxide films from 8.6 to 57 nm lead to an increase in hysteresis width. Thicker films develop two different slopes (steep and gradual) when cooling through the metal-insulator transition, where the steep transition matches that of the heating cycle of the transition. This asymmetry in the hysteresis is apparent and similar in both the electrical and optical measurements. Temperature-dependent Raman spectroscopy and temperature-dependent x-ray diffraction confirm the same anomaly suggesting a structural dependence on hysteretic shape. Transmission electron microscopy identifies texturing and faceting in-plane, especially along the surface of these films, and confirms the x-ray diffraction data. Identifying this facet texturing is valuable for film growth as well as for applications, such as logic and memory systems, that utilize the hysteretic nature of vanadium dioxide.



## 1. Introduction

The reversible phase change of vanadium dioxide ($VO_2$) provides significant opportunities as an optical material. Bulk $VO_2$ has a metal-to-insulator phase transition temperature of 68°C, which makes it accessible from room temperature, and additionally doped and strained thin films and nanocrystals have decreased this transition temperature to room temperature [1]. Thus, the large variation in optical properties (metal and insulator) of $VO_2$ are used in many applications, one example is thermal sensing smart windows and passive thermal control [2,3]. Also, this phase change is hysteretic with temperature enabling a host of other applications, such as optical modulation, switching and memory [4,5].

The measured transition properties of $VO_2$ vary widely and can depend on growth technique, crystal size (nanoparticles, thin-film, bulk, etc.), annealing, doping, strain, and other factors. In general, the properties of the hysteresis are widely unknown, which is not surprising since controversy remains over the origin of the transition [6]. Early work suggested that vacancies could cause hysteresis by interrupting long-range optical phonons [7]. In addition, crystallite grain size and stress were correlated with hysteresis width [8], where stress was composed of two terms: external (thermal expansion mismatch in film and substrate) and internal (voids, grain boundaries, etc.).

More recent research still links hysteresis to crystal quality and strain. These explanations, however, can be contradictory: some explain that high-quality crystals resulted in narrow hysteresis [9,10], and others explained a high-quality crystal resulted in a wide hysteresis [11–13]. The experimental evidence in the former show that increasing crystal quality (larger grain size, fewer defects) decreased the hysteresis width while increasing transition amplitude

#371349 https://doi.org/10.1364/OME.9.003717
Journal © 2019 Received 1 Jul 2019; revised 9 Aug 2019; accepted 9 Aug 2019; published 15 Aug 2019

Optical Materials EXPRESS

and sharpness [9,10]. While the latter groups used $VO_2$ nanoparticles and nanoprecipitates to show that decreasing nanocrystal size produced a wider hysteresis (along with decreased transition amplitude) [11–13]. In this latter group, the smaller $VO_2$ nanocrystals were described as higher quality crystals which suggested that fewer defects in these smaller crystals widen the hysteresis by limiting the available nucleation sites for the phase transition [11]. However, these results were limited to $VO_2$ nanoparticles, and therefore do not provide information on epitaxial integration or more ordered structures which could influence a structural transition, and additionally nanoparticle results do not provide information for thin film applications (such as Mott transistors, etc.). Recently, some groups have even used nanostructure geometries to modify the hysteresis [14].

In addition, the question of stoichiometry and crystal quality were addressed by annealing thin $VO_2$ films, which also produced disparate results. One group showed that oxidation conditions (0.01-0.25 Torr) during annealing produced a more abrupt transition with a narrow hysteresis with compact and highly oriented $VO_2$ grains [15]. This group explained their narrow hysteresis was due to larger crystallites. However, another group demonstrated thermal annealing resulted in a wider hysteresis due to similar grain growth and improved crystallinity with the larger, more crystalline grains [5]. Counter to the previous claim, the latter experiment was explained by competing effects of crystallinity and grain size, where the (previous) larger volume crystallites (not annealed) have a greater probability of finding a nucleating defect that would decrease the hysteresis [5].

To investigate the transition properties further while minimizing the effects of the crystal stoichiometry and inhomogeneity, micro-Raman spectroscopy was performed on $VO_2$ samples. As in previous research, the results show opposite conclusions with respect to the hysteresis width of the transitions. One group showed a narrower hysteresis width when comparing a more crystalline bulk sample to that of a thin film sample [16]. Another group demonstrated that isolated $VO_2$ nanoparticles had a wider hysteresis than a thin film due to fewer nucleation sites within the nanoparticles [17].

Other plasmonic and nonlinear-optical methods have been employed in an attempt to understand the hysteresis in $VO_2$. Plasmonic split-ring resonators interrogated the $VO_2$ hysteresis and demonstrated broadened widths with reduced probing volume, suggesting fewer phase transition nucleation sites [18]. While a nonlinear optical investigation (third-harmonic generation) suggest hysteresis width is due to nanocrystal inhomogeneities [19].

To complicate matters further, some experimental optical data have shown an asymmetric hysteresis, and one work previously noted an asymmetric hysteresis in optical transmittance and electrical resistance [20]. In some of these works, the transition upon cooling shows multiple distinct slopes: a slope at the higher-temperature portion of the transition that matches the slope observed during heating and a more gradual slope during the lower-temperature portion of the transition. These are most apparent in optical measurements such as infrared emittance [21,22], optical constants measured via spectroscopic ellipsometry [23], optical transmittance and reflectance [5,8,20,24], and Raman spectroscopy [25]. Several of these experimental works exhibited similar hysteresis asymmetry for film thicknesses from 30 nm [21] to 80 nm [23] to 190 nm [22], and were grown by different methods (pulsed laser deposition and rf sputtering). However, this hysteresis asymmetry is often less obvious in electrical resistivity measurements since the logarithm of the resistivity is generally plotted, which tends to flatten the multiple slopes.

In addition to these experimental efforts, several theories have been suggested to describe the transition hysteresis. Many rely on the hysteresis properties as a strong function of crystal properties (crystallite size, grain boundaries, defect density, etc.). One qualitative model revealed several transitional correlations, including: transition temperature proportional to crystal strain; transition slope inversely proportional to defect density; transition amplitude

Optical Materials EXPRESS

inversely proportional to defect density; and hysteresis width proportional to interfacial energy and inversely proportional to critical radius [26]. While another report used a charge-transfer model to demonstrate how increasing elastic defects (vacancies and grain boundaries) increases hysteresis width [10]. Still others have described the phase transition as a percolation transition and used an effective-medium approximation [20,27–31].

Only a few models were capable of predicting an asymmetry in the hysteresis. In one model, an asymmetric hysteresis was created by grain-size dependent phase equilibrium temperature variations and oxygen nonstoichiometry, which resulted in more gradual slopes during cooling [32]. Another technique explained the resistive asymmetric hysteresis with a random resistor network for the interconnected network of polycrystalline regions [33]. Finally, another modeled an asymmetric hysteresis loop by summing of individual "elementary" nanocrystallites, each with discrete hysteresis and phase equilibrium temperatures [34]. However, the theory of $VO_2$ nanocrystallites is more useful in powder studies, with possible application to sol gel or sputtered materials, while these models may not provide an accurate model for more ordered structures and how that impacts the phase transition.

This paper investigates the gap in understanding of the hysteretic transition by growing a series of $VO_2$ films with varying thicknesses. All films, 8.6 to 57 nm in thickness, were grown by atomic-layer deposition (ALD) on sapphire substrates and atomic force microscopy (AFM) was used to characterize film morphology. The temperature dependence of the electrical resistance as well as optical transmittance and reflectance were measured. To correlate these with structural properties the temperature dependence of the Raman and x-ray diffraction spectra were also measured. Our results suggest that facet texturing of the thicker films could be responsible for the in-plane response, which produces a bi-modal asymmetry in the hysteresis. This is supported by additional TEM analysis.

## 2. ALD growth

Amorphous $VO_2$ was deposited on c-plane sapphire substrates by ALD in an Ultratech Savannah 200 reactor at 150°C using tetrakis(ethylmethyl)amido vanadium (TEMAV) and ozone precursors with a saturated growth rate of approximately 0.9Å/cycle [35]. The vanadium precursor was chosen since it is in the + 4 oxidation state and promotes the preferential formation of the $VO_2$ phase. It has been established that anneal is more critical than growth [36], thus, the as-deposited $VO_2$ films were crystallized with an ex-situ anneal at 475°C in $5 \times 10^{-5}$ Torr of oxygen for 1–2 hours depending on film thickness. Six different thickness were grown: 8.6, 12.5, 18, 30, 44, and 57 nm. After annealing, micro-Raman spectroscopy confirmed the correct $VO_2$ phase and ensured the fabrication process resulted in structurally similar films.

AFM images were obtained for all the samples using the same scan conditions and image size for accurate comparison of film roughness. These data show that the particle size seems similar across samples, and that there appears to be no trend in roughness with film thickness (see Fig. 1), except that films less than 20 nm have a larger roughness. To examine the influence of roughness, the variation of film thickness due to the roughness is shown in Fig. 1(c). For the two thinnest films, Fig. 1(c) shows the roughness variation can be as large as the thickness itself for the 8.6- and 12.5-nm films, and for the 18-nm film there can be >100% thickness variations.

Optical Materials EXPRESS

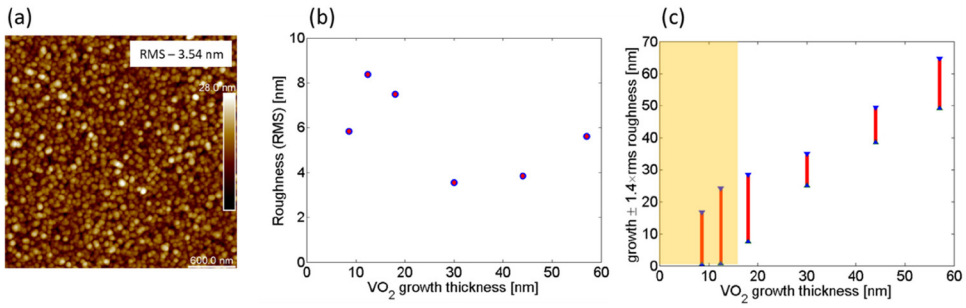


**Fig. 1.** (a) Atomic force microscopy of a 30-nm $VO_2$ film shows a 3.54-nm (rms) surface roughness. (b) the surface roughness measured by AFM as a function of film thickness. (c) Film thicknesses range was calculated as ± 1.4x rms roughness plotted vs. average grown film thickness.

## 3. Optical characterization

Temperature-dependent optical transmittance and reflectance of the films were collected with a spectrally broad source using a coarse temperature (10°C) spacing, Fig. 2(a), as well as at a single wavelength (1550 nm) with increased temperature resolution (<1°C) to better observe the optical hysteresis, Fig. 2(b). The largest change in optical transmittance and reflectance occurred in the infrared as seen in Fig. 2(a). There was also an interesting change observable in the visible region where the optical transmittance and reflectance undergo a small change that is opposite to the changes in the infrared. In Fig. 2(b), the phase transition slope during heating gets a little steeper as the thickness increases from 8.6 to 30 nm. An asymmetry in the hysteresis was observed in the thickest (44- and 57-nm) films, which showed the sharpest insulator-to-metal transition upon heating, but upon cooling (metal-to-insulator transition) began with a steep slope and then changed to a second more gradual slope.

The transition properties were determined by fitting the data using several schemes (all of which agreed), however, the Gaussian method worked best on the multiple transition slopes of the thickest sample. A Gaussian fit to the derivative of the optical data provided the transition temperature (Gaussian peak) and transition steepness (ΔT, Gaussian width—FWHM). Analysis of the optical properties of the transition are plotted in Figs. 2(c)–2(e) and showed the transition temperature (both during heating and cooling) slightly decreased with increasing thickness, except for the thickest sample which deviated from the trend resulting in an increased transition temperature only upon heating (insulator-to-metal transition). This deviation is not surprising since the thickest sample also produced a marked increase in hysteresis width, Fig. 2(e).

As sample thickness increased the transition also became steeper (narrower transition, ΔT), as shown in Fig. 2(d). While the transition during cooling was slightly steeper than during heating for the thinner samples this switched for the thicker samples (44 and 57 nm), i.e., a slightly steeper transition during heating (insulator-to-metal transition)—although the 57-nm-thick sample has two slopes during cooling: one more steep and one less steep than the heating transition. These measurements led to an optical hysteresis width, Fig. 2(e), that slightly decreased with increasing sample thickness (from 8 to 44 nm), followed by a rapid hysteresis increase with a pronounced asymmetry for the thickest (57-nm) sample.

Optical Materials EXPRESS

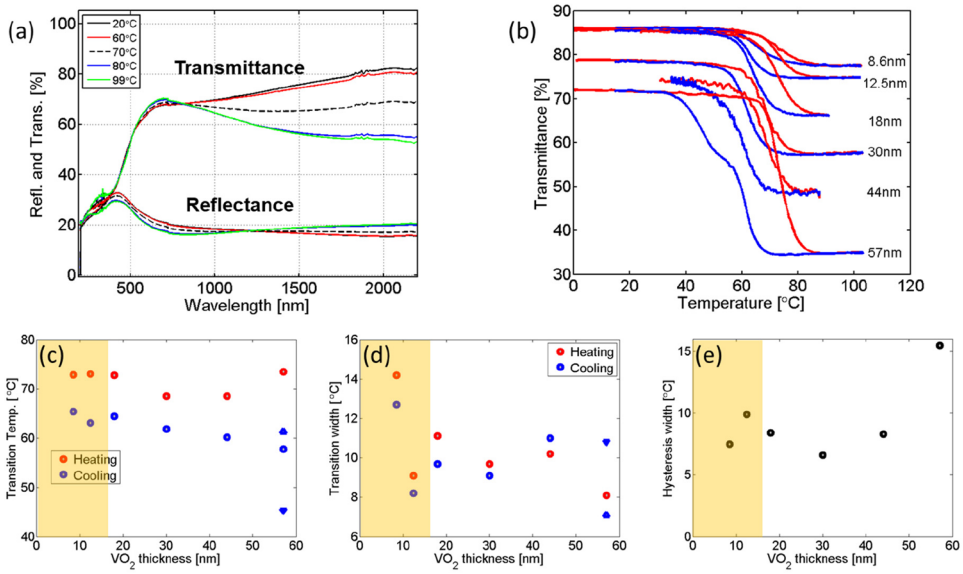


**Fig. 2.** (a) Temperature-dependent optical reflectance and transmittance spectra for the 30-nm $VO_2$ film thickness for temperatures of 20, 60, 70, 80, and 99°C. (b) Optical transmittance at 1550nm for 8.6, 12.5, 18, 30, 44, and 57-nm $VO_2$ film thicknesses shows the hysteretic nature of the transition (red: heating, blue: cooling). Measured (c) transition temperature and (d) transition width during heating and cooling for each thickness (with two widths measured upon cooling for the 57-nm sample due to the two distinct slopes when cooling). (e) The calculated hysteresis width plotted as a function of film thickness.

## 4. Electrical characterization

To determine if similar changes occur in the electrical response to the phase transition, Ti/Au contacts were patterned in a circular transmission line model geometry [37] to measure the resistivity across a 2-μm gap. The temperature-dependent resistance was measured for the same series of $VO_2$ thicknesses, shown in Fig. 3(a). The resistance exhibited a similar behavior to the optical observations of Fig. 2, where the slope of the resistance during the heating transition gets steeper as the thickness increases from 8.6 to 30 nm, and the 57-nm film shows the steep transition upon heating but two slopes (steep, then gradual) upon cooling.

While the optical characterization tends to probe the bulk material, the electrical characterization can be more sensitive to the surface properties. For the thinnest films (8.6 and 12.5 nm) the surface roughness was large enough (see Fig. 1) to potentially have regions without $VO_2$, and this could explain the similar higher resistances of these films. The resistance decreased as the film thickness increased until the thickest (57-nm) film. For this thickest film not only did the resistance increase, but the hysteresis widened and became noticeably asymmetric.

Most groups commonly characterize the transition using the logarithm of the resistance (as opposed to linear resistance) as a function of temperature [9]. Compared to the optical data, the electrical resistance data show similar dependences of transition temperature, steepness, and hysteresis width as a function of thickness. While the trends are similar for optical and electrical measurements, there are some notable differences. The most obvious difference was the higher transition temperature of the electrical data, for example in the 30-nm-thick film the electrical transition occurred at 75.4°C versus 68.6°C for the optical transition. This may be due to the logarithm of the data, since for this type of waveform the logarithm will move the point of inflection to higher values.

Optical Materials EXPRESS

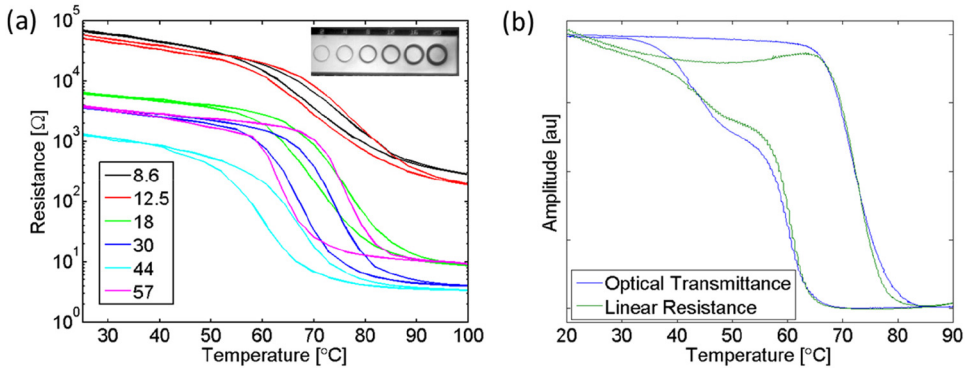


**Fig. 3.** (a) Temperature-dependent electrical resistance for 8.6, 12.5, 18, 30, 44, and 57-nm $VO_2$ film thicknesses measured using circular transmission line model contact, as shown in inset. (b) Normalized optical transmittance (blue) and normalized electrical resistance (green) measured on the 57-nm-thick sample show similar asymmetric features. Note: the resistance in (b) is plotted on a linear scale with slope correction applied to remove the linear temperature-dependent resistance of the insulating phase.

Recalculating transition temperatures using the linear data were much closer to the optical data. However, the linear resistance data are more challenging since there is a large (somewhat linear) temperature dependence in the insulating state. The influence of the temperature dependence in the insulating phase is dramatically reduced to an insignificant slope in the logarithmic plots, due to the orders-of-magnitude resistance change at the transition temperature. However, using linear resistance data brought the transition properties in better agreement with the optical data. For example, in the 30-nm-thick film the electrical transition of 75.4°C using a log scale was reduced to 67.6°C when using a linear scale, thereby providing much closer agreement with the 68.6°C for the optical transition while maintaining a similar hysteresis width (6.8°C versus 6.3°C). When examining the linear resistance data, the properties were calculated from a fit with two-Gaussians. As with the optical data, the cooling data exhibited a noticeable second slope at lower temperatures. This second slope was hard to resolve amidst the large temperature-dependent resistance of the insulating phase, but was strong in the thickest sample and compared favorably with the second slope of the optical data, see Fig. 3(b).

## 5. Crystal structure

### *Raman spectroscopy*

Since both the electronic and optical measurements showed similar trends with increasing thickness, temperature-dependent Raman spectroscopy was performed on the samples.. The samples were excited with a 532-nm source, and Raman spectra were recorded while both heating and cooling the sample through the metal-insulator transition, as shown in Fig. 4. The excitation power level was reduced by 100 times to ensure laser-induced sample heating was insignificant. Gaussian functions provided a good fit to the spectral peaks, and quantified the peak Raman intensity as a function of temperature, as shown for select $VO_2$ Raman peaks in Fig. 4. These data showed similar trends to the previous electrical and optical data, and the thickest, 57-nm, $VO_2$ film exhibited a significant asymmetry in Raman response thereby suggesting a possible structural link to this behavior.

For the thickest sample, the temperature dependence of all the resolvable Raman $A_g$ modes of the monoclinic (insulating) $VO_2$ exhibited two distinct slopes upon cooling, similar to that of the optical and electrical data for the 57-nm-thick sample. The Raman peaks at 190, 220,

Optical Materials EXPRESS

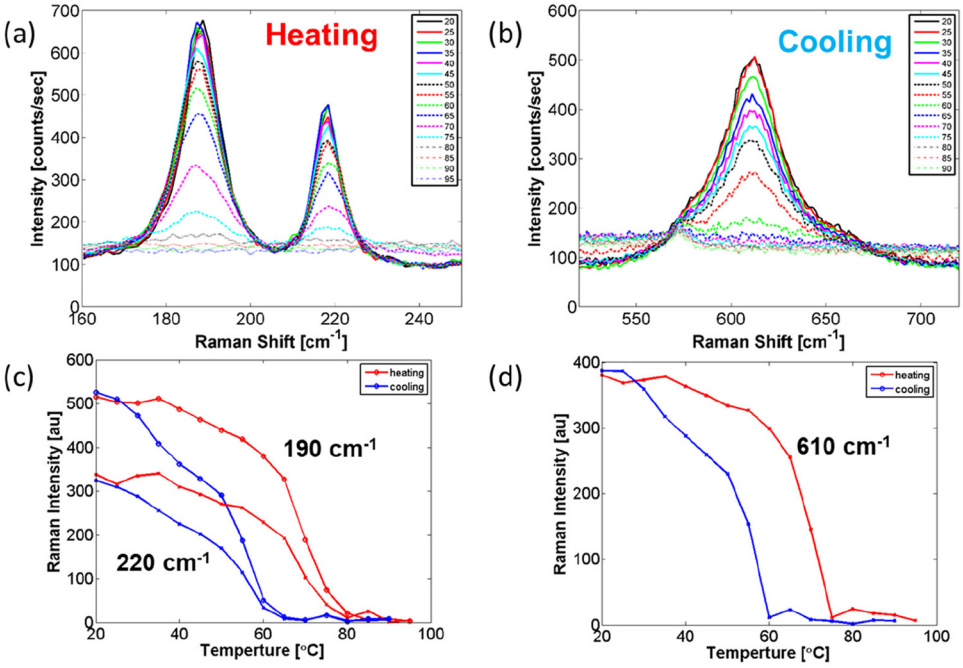


**Fig. 4.** Raman $A_g$ modes at (a) 190 and 220cm$^{-1}$, and (b) 610 cm$^{-1}$ measured as a function of temperature for a 57-nm thick $VO_2$ film. Gaussian fits to the spectral peaks (c) and (d) show the Raman intensity varies as a function of temperature similar to the electrical and optical data, with two distinct slopes upon cooling, suggests a structural link to this behavior.

and 610 cm$^{-1}$ had the best signal-to-noise ratio to resolve these features, as shown in Figs. 4(c) and 4(d). Throughout the temperature range, the energy of Raman modes (not shown) did not exhibit any significant change, however, the linewidth (also not shown) of the 190- and 220-cm$^{-1}$ modes increased monotonically by ~20% with increasing temperature while the linewidth of the 610-cm$^{-1}$ mode did not change.

The intensity of the $A_g$ modes exhibited a gradual decrease with increasing temperature and then a dramatic decrease to zero at the insulator-to-metal transition near 70°C. This slight decrease in Raman intensity prior to the phase transition during heating was unexpected, but has been observed before [16], and was uncorrelated with the optical transmittance and electrical resistance data. Upon cooling, a similar rapid increase in the Raman intensity is observed at the metal-to-insulator transition (near 55°C) followed by a gradual increase in Raman intensity as temperatures decreased further from 55 to 30°C, but, this gradual second slope is steeper than the more gradual slope observed during heating. This asymmetric hysteresis of the Raman intensity qualitatively matched that of the electrical and optical data with a rapid change at both phase transition points, and then a more gradual change upon cooling from 50-30°C.

### *X-ray diffraction and TEM*

To further examine the structure, temperature-dependent x-ray diffraction was performed on a thick sample with asymmetric hysteresis. Two techniques were used: 1) normal incidence x-ray diffraction (XRD), shown Fig. 5(a), and 2) grazing incidence x-ray diffraction (GIXRD) with Cornell's High Energy Synchrotron Source, shown Fig. 5(b). The GIXRD characterized the in-plane structure which is not well studied. Normal incidence out-off plane XRD measurements of $VO_2$ layers were measured using a Rigaku system that employs a rotating Cu anode to produce

Optical Materials EXPRESS

Cu-$K_\alpha$ radiation. The sample temperature was modified by circulating ethylene glycol through the sample holder, and controlled to ± 1°C by monitoring a RTD that was mounted on the sample holder adjacent to the $VO_2$ sample. For GIXRD measurements, 10.18-keV photons were generated by a synchrotron light source at the G2 line of Cornell's High Energy Synchrotron Source, and the sample temperature was measured using a thermocouple mounted on the surface of the film. Combining these data (XRD and GIXRD) enabled observation of both the in-plane and out-of-plane features of the $VO_2$.

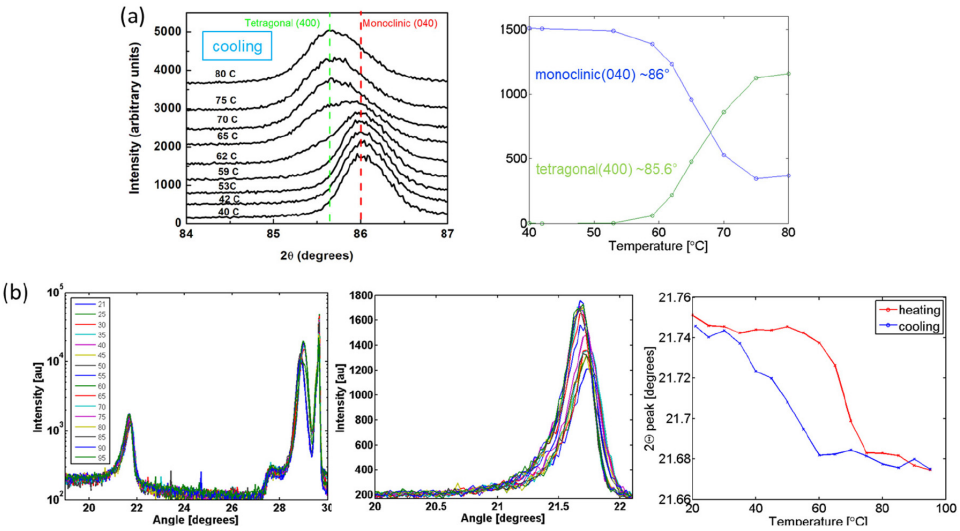


**Fig. 5.** Temperature-dependent (a) normal-incidence XRD showed a metal-insulator transition, with Gaussian-fit out-of-plane peaks, from 85.6 degree peak, tetragonal (400), to the 86 degree peak, monoclinic (040). (b) GIXRD measured the in-plane peaks. The in-plane 21.868-degree peak gradually shifts to the 21.7757 degrees, similar to the more gradual optical and electrical transition upon cooling.

The second-order XRD peaks, shown in Fig. 5(a), provided a clear separation of the two out-of-plane peaks from the insulating, monoclinic (040) and metallic, tetragonal (400) phases. Performing these temperature-dependent XRD measurements showed the reversible transition from monoclinic to tetragonal and back. The data also showed that the ALD $VO_2$ is a highly oriented polycrystalline film. The peak locations showed the room-temperature orientations were aligned (040)//(0001), similar to $VO_2$ films grown by several methods [38]. These curves followed the hysteresis typical in these materials, but did not show any structure related to the asymmetry in the hysteresis, i.e., the additional slope at lower temperature during cooling.

The GIXRD diffraction data showed several peaks revealing a more textured film in-plane, see Fig. 5(b). Most in-plane peaks exhibited similar transitions to out-of-plane peaks. For example, the monoclinic (200), $P2_1/c$(14) peak (PDF card number: 01-076-0456) rapidly shifted from 28.8 to the tetragonal (011), $P4_2/mnm$(136) peak (PDF card number: 00-044-0253) at 29 degrees when heating between 60 to 70°C, and then shifted back from 29 to 28.8 degrees upon cooling between 65 to 55°C. However, the data near 22 degrees showed a transition from the monoclinic (011) oriented planes at 21.74 degrees (relaxed location at 21.868 degrees) to the tetragonal (110) peak at 21.68 degrees (relaxed location at 21.7757 degrees). The temperature-dependent shift in this peak was interesting since it showed only the more gradual sloped hysteresis during cooling at lower temperatures (50-30°C). The sapphire peak showed no significant changes, thereby verifying the changes were due only to the temperature-dependent $VO_2$ phase change. This demonstrates there was a physical structure associated with this asymmetric anomaly in the

Optical Materials EXPRESS

hysteresis which arises from the misorientation and texturing of the thickest ALD grown $VO_2$ films.

Finally, TEM imaging was performed. A Focused Ion beam (FIB) was used to prepare cross-sectional samples of $VO_2/Al_2O_3$ (0002). The process involves the use of an *in-situ* lift-out technique to prepare electron transparent lamellae. High resolution as well as low-resolution phase contrast TEM images were obtained using JEOL 2010F and Analytical FEI Tecnai G2 F20 ST FE-TEM both operating at 200kV and equipped with a Schottky field emission source with a focused probe of 0.2nm and point-to-point resolution of 0.19 nm. The sample stage was cooled with liquid nitrogen and stabilized to a temperature of 150K. Selected area diffraction patterns were processed using fast Fourier transform imaging and post-data-acquisition analytical techniques to index the diffraction pattern reflections as well as in the determination of the crystallographic orientation relationship between $VO_2$ film and sapphire substrate.

Cross-sectional high-resolution transmission electron microscopy (HRTEM) images of (020) – oriented monoclinic $VO_2$ ($P2_1/c$) on (0002) *c*-plane oriented $Al_2O_3$ substrates were obtained as shown in Fig. 6. The out-of-plane crystallographic orientation relationship between $VO_2$ and $Al_2O_3$ was determined to be $[020]VO_2$// $[0001]Al_2O_3$ and $(200)VO_2$// $(01\bar{1}0)Al_2O_3$, while the in-plane orientation relationship for the same set of samples was $[200]VO_2$// $[\bar{2}\bar{1}10]Al_2O_3$ and $(020)VO_2$// $(0002)Al_2O_3$. This confirms the orientations established in the XRD measurements. The interfacial crystal structures showed an abrupt interface suggesting a high quality low-defect $VO_2$ crystal structure. In addition, there was evidence of texturing resulting in a high density of parallel low-surface free energy facetted planes parallel to {220} with low density of unsatisfied bonds or point defects. Thus, this noticeable texturing supports the GIXRD observations, where the lower temperature transition of the in-plane (110) planes suggests a structural explanation for the wider hysteresis and appearance of a second slope when cooling through the metal-insulator transition.

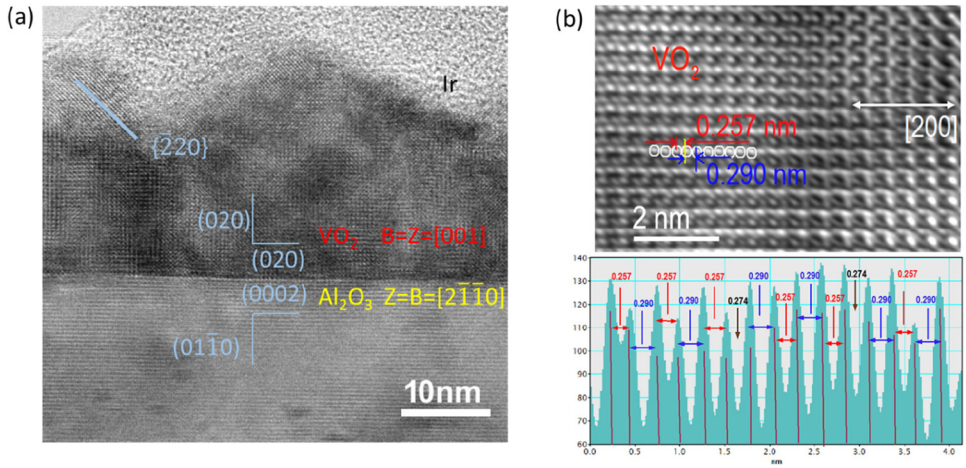


**Fig. 6.** High resolution transmission electron microscopy reveals crystal structure of (a) oriented monoclinic $VO_2$ ($P2_1/c$) on (0002) c-plane oriented $Al_2O_3$ substrates with facetted planes parallel to {220}. (b) a line profile taken on the image showed alternating V-V bond lengths of 0.257 and 0.290 nm along [002] crystallographic orientation.

The high resolution images indicate lattice constants of $a_{m1}$=0.576 nm and $c_{m1}$=0.528 nm which agrees with the reported low temperature (monoclinic) $VO_2$ phase with a point symmetry of $P2_1/c(14)$ with theoretical lattice constants of $a_{m1}$ = 0.575nm and $c_{m1}$=0.538 nm. This was independent verification which confirmed the results obtained from our GIXRD measurements. In addition, a line profile taken on the inverse fast Fourier transform of HRTEM image, Fig. 6(b),

Optical Materials EXPRESS

showed alternating V-V bond lengths of 0.257 and 0.290 nm along [002] crystallographic orientation. The observation of these alternating vanadium bond lengths were similar to Goodenough's formalism [7] of the vanadium dimer which forms in the insulating, monoclinic $VO_2$ ($P2_1/c$) phase.

## 6. Conclusion

We explored the thermal hysteresis in the metal-insulator phase transition in vanadium dioxide. We compared historical work in the literature as well as experimental work by a comprehensive suite of fabrication and measurement techniques. ALD $VO_2$ films with thicknesses from 8.6 to 57 nm were grown on c-$Al_2O_3$ to identify the thickness-dependent hysteretic behavior. The hysteresis properties were correlated in temperature-dependent optical and electrical measurements, namely, as the film thickness increased the transition temperature showed a slight decrease and the transition steepness increased with increasing temperature, except for the thickest films (44- and 57-nm thicknesses). The hysteresis width remained nearly the same except for the thickest (57-nm) samples, but an asymmetry in the hysteresis was observed. This asymmetry manifested itself in the cooling (metal-to-insulator) transition by initially following the steep transition, but then (from 50-30°C) changed to a more gradual slope. Similar hysteresis asymmetries were found in the literature for a variety of $VO_2$ samples but failed to identify the cause of this phenomenon.

To investigate the origin of this asymmetry in our 57-nm-thick sample, temperature-dependent Raman, XRD, GIXRD, and TEM measurements were performed. The Raman $A_g$ modes exhibited a similar asymmetry, similar to the optical and electrical measurements, potentially indicating a structural mechanism. While out-of-plane XRD measurements did not show this asymmetry, the GIXRD revealed the presence of a temperature-dependent asymmetry between the in-plane (110) tetragonal $P4_2/mnm(136)$ and the (011) monoclinic $P2_1/c(14)$ phases in the same lower temperature region (50-30°C), matching the optical and electrical asymmetry. Finally, TEM imaging showed the presence of the (220) plane faceting which further explains the GIXRD results. Thus, we conclude that our observations have a foundation in the physical structure of the $VO_2$ since the hysteresis asymmetry for the thicker samples was observed in both the electrical and optical measurements (sensitive to lateral/surface and volume/bulk properties, respectively) and correlate with similar temperature dependent structural properties (observed in Raman and XRD).

These results show that for thicker ALD grown films texturing can produce unique transition properties, e.g., the insulator-to-metal transition is rapid while the metal-to-insulator transition is a two-step process. Texturing was previously identified in $VO_2$ samples, but it was not associated with an asymmetric hysteresis [39,40]. Klimov et al. explain that bimodal size distributions can lead to jumps in the hysteresis [32]. These jumps are similar to what we observed in our thickest sample, and we showed this could be a manifestation of texturing. Engineering the hysteretic properties is useful in applications of $VO_2$ and other phase transition materials, such as memory and logic elements.

## Funding

Office of Naval Research.

## References

1. X. Tan, T. Yao, R. Long, Z. Sun, Y. Feng, H. Cheng, X. Yuan, W. Zhang, Q. Liu, C. Wu, Y. Xie, and S. Wei, "Unraveling Metal-insulator Transition Mechanism of $VO_2$ Triggered by Tungsten Doping," Sci. Rep. **2**(1), 466 (2012).
2. S. M. Babulanam, T. S. Eriksson, G. A. Niklasson, and C. G. Granqvist, "Thermochromic $VO_2$ films for energy-efficient windows," Sol. Energy Mater. **16**(5), 347–363 (1987).

Optical Materials EXPRESS


3. M. Benkahoul, M. Chaker, J. Margot, E. Haddad, R. Kruzelecky, B. Wong, W. Jamroz, and P. Poinas, "Thermochromic $VO_2$ film deposited on Al with tunable thermal emissivity for space applications," Sol. Energy Mater. Sol. Cells **95**(12), 3504–3508 (2011).
4. R. F. Haglund, S. M. Weiss, and K. Appavoo, "Photonic and plasmonic modulators based on optical switching in $VO_2$," Proc. SPIE **9370**, 93701C (2015).
5. J. Y. Suh, R. Lopez, L. C. Feldman, and R. F. Haglund, "Semiconductor to metal phase transition in the nucleation and growth of $VO_2$ nanoparticles and thin films," J. Appl. Phys. **96**(2), 1209–1213 (2004).
6. J. H. Park, J. M. Coy, T. S. Kasirga, C. Huang, Z. Fei, S. Hunter, and D. H. Cobden, "Measurement of a solid-state triple point at the metal-insulator transition in $VO_2$," Nature **500**(7463), 431–434 (2013).
7. J. B. Goodenough, "The two components of the crystallographic transition in $VO_2$," J. Solid State Chem. **3**(4), 490–500 (1971).
8. F. C. Case, "Modifications in the phase transition properties of predeposited $VO_2$ films," J. Vac. Sci. Technol., A **2**(4), 1509–1512 (1984).
9. D. Brassard, S. Fourmaux, M. Jean-Jacques, J. C. Kieffer, and M. A. E. Khakani, "Grain size effect on the semiconductor-metal phase transition characteristics of magnetron-sputtered $VO_2$ thin films," Appl. Phys. Lett. **87**(5), 051910 (2005).
10. V. S. Vikhnin, S. Lysenko, A. Rua, F. Fernandez, and H. Liu, "The model of metal–insulator phase transition in vanadium oxide," Phys. Lett. A **343**(6), 446–453 (2005).
11. T. Jostmeier, J. Zimmer, H. Karl, H. J. Krenner, and M. Betz, "Optically imprinted reconfigurable photonic elements in a $VO_2$ nanocomposite," Appl. Phys. Lett. **105**(7), 071107 (2014).
12. R. Lopez, T. E. Haynes, L. A. Boatner, L. C. Feldman, and R. F. Haglund, "Size effects in the structural phase transition of $VO_2$ nanoparticles," Phys. Rev. B **65**(22), 224113 (2002).
13. R. Lopez, L. A. Boatner, T. E. Haynes, L. C. Feldman, and R. F. Haglund, "Synthesis and characterization of size-controlled vanadium dioxide nanocrystals in a fused silica matrix," J. Appl. Phys. **92**(7), 4031–4036 (2002).
14. X. Li, S. Zhang, L. Yang, X. Li, J. Chen, and C. Huang, "A convenient way to reduce the hysteresis width of $VO_2$(M) nanomaterials," New J. Chem. **41**(24), 15260–15267 (2017).
15. S. Yu, S. Wang, M. Lu, and L. Zuo, "A metal-insulator transition study of $VO_2$ thin films grown on sapphire substrates," J. Appl. Phys. **122**(23), 235102 (2017).
16. G. I. Petrov, V. V. Yakovlev, and J. Squier, "Raman microscopy analysis of phase transformation mechanisms in vanadium dioxide," Appl. Phys. Lett. **81**(6), 1023–1025 (2002).
17. E. U. Donev, R. Lopez, L. C. Feldman, and R. F. Haglund, "Confocal Raman Microscopy across the Metal−Insulator Transition of Single Vanadium Dioxide Nanoparticles," Nano Lett. **9**(2), 702–706 (2009).
18. K. Appavoo and R. F. Haglund, "Detecting Nanoscale Size Dependence in VO2 Phase Transition Using a Split-Ring Resonator Metamaterial," Nano Lett. **11**(3), 1025–1031 (2011).
19. G. I. Petrov, V. V. Yakovlev, and J. A. Squier, "Nonlinear optical microscopy analysis of ultrafast phase transformation in vanadium dioxide," Opt. Lett. **27**(8), 655–657 (2002).
20. J. Rozen, R. Lopez, R. F. Haglund, and L. C. Feldman, "Two-dimensional current percolation in nanocrystalline vanadiumdioxide films," Appl. Phys. Lett. **88**(8), 081902 (2006).
21. A. Hendaoui, N. Émond, M. Chaker, and É Haddad, "Highly tunable-emittance radiator based on semiconductor-metal transition of $VO_2$ thin films," Appl. Phys. Lett. **102**(6), 061107 (2013).
22. G. Leahu, R. L. Voti, C. Sibilia, and M. Bertolotti, "Anomalous optical switching and thermal hysteresis during semiconductor-metal phase transition of $VO_2$ films on Si substrate," Appl. Phys. Lett. **103**(23), 231114 (2013).
23. J. B. Kana Kana, J. M. Ndjaka, G. Vignaud, A. Gibaud, and M. Maaza, "Thermally tunable optical constants of vanadium dioxide thin films measured by spectroscopic ellipsometry," Opt. Commun. **284**(3), 807–812 (2011).
24. K. J. Miller, K. A. Hallman, R. F. Haglund, and S. M. Weiss, "Silicon waveguide optical switch with embedded phase change material," Opt. Express **25**(22), 26527–26536 (2017).
25. X. Wang, Z. Gong, K. Dong, S. Lou, J. Slack, A. Anders, and J. Yao, "Tunable Bragg filters with a phase transition material defect layer," Opt. Express **24**(18), 20365–20372 (2016).
26. J. Narayan and V. M. Bhosle, "Phase transition and critical issues in structure-property correlations of vanadium oxide," J. Appl. Phys. **100**(10), 103524 (2006).
27. H. S. Choi, J. S. Ahn, J. H. Jung, T. W. Noh, and D. H. Kim, "Mid-infrared properties of a $VO_2$ film near the metal-insulator transition," Phys. Rev. B **54**(7), 4621–4628 (1996).
28. J. D. Frame, N. G. Green, and X. Fang, "Modified Maxwell Garnett model for hysteresis in phase change materials," Opt. Mater. Express **8**(7), 1988–1996 (2018).
29. P. J. Hood and J. F. DeNatale, "Millimeter-wave dielectric properties of epitaxial vanadium dioxide thin films," J. Appl. Phys. **70**(1), 376–381 (1991).
30. L. A. L. de Almeida, G. S. Deep, A. M. Nogueira-Lima, and H. Neff, "Modeling of the hysteretic metal-insulator transition in a vanadium dioxide infrared detector," Opt. Express **41**(10), 2582–2589 (2002).
31. L. A. L. de Almeida, G. S. Deep, A. M. N. Lima, I. A. Khrebtov, V. G. Malyarov, and H. Neff, "Modeling and performance of vanadium–oxide transition edge microbolometers," Appl. Phys. Lett. **85**(16), 3605–3607 (2004).
32. V. A. Klimov, I. O. Timofeeva, S. D. Khanin, E. B. Shadrin, A. V. Ilinskii, and F. Silva-Andrade, "Hysteresis loop construction for the metal-semiconductor phase transition in vanadium dioxide films," Tech. Phys. **47**(9), 1134–1139 (2002).

Optical Materials EXPRESS


33. J. Dai, X. Wang, Y. Huang, and X. Yi, "Modeling of temperature-dependent resistance in micro- and nanopolycrystalline $VO_2$ thin films with random resistor networks," Opt. Eng. **47**(3), 033801 (2008).
34. E. B. Shadrin, A. V. Il'inskiĭ, A. I. Sidorov, and S. D. Khanin, "Size effects upon phase transitions in vanadium oxide nanocomposites," Phys. Solid State **52**(11), 2426–2433 (2010).
35. M. Currie, M. A. Mastro, and V. D. Wheeler, "Characterizing the tunable refractive index of vanadium dioxide," Opt. Mater. Express **7**(5), 1697–1707 (2017).
36. P. A. Premkumar, M. Toeller, I. P. Radu, C. Adelmann, M. Schaekers, J. Meersschaut, T. Conard, and S. Van Elshocht, "Process study and characterization of $VO_2$ thin films synthesized by ALD using TEMAV and O3 precursors," ECS J. Solid State Sci. Technol. **1**(4), P169–P174 (2012).
37. G. S. Marlow and M. B. Das, "The effects of contact size and non-zero metal resistance on the determination of specific contact resistance," Solid-State Electron. **25**(2), 91–94 (1982).
38. H. Kim, N. Charipar, M. Osofsky, S. B. Qadri, and A. Piqué, "Optimization of the semiconductor-metal transition in $VO_2$ epitaxial thin films as a function of oxygen growth pressure," Appl. Phys. Lett. **104**(8), 081913 (2014).
39. C. Petit, J.-M. Frigerio, and M. Goldmann, "Hysteresis of the metal-insulator transition of $VO_2$; evidence of the influence of microscopic texturation," J. Phys.: Condens. Matter **11**(16), 3259–3264 (1999).
40. M. E. Uslu, I. B. Misirlioglu, and K. Sendur, "Selective IR response of highly textured phase change $VO_2$ nanostructures obtained via oxidation of electron beam deposited metallic V films," Opt. Mater. Express **8**(8), 2035–2049 (2018).